Observing Dynamical Currents in a Non-Hermitian Momentum Lattice

Rodrigo Rosa-Medina,[1] Francesco Ferri,[1] Fabian Finger,[1] Nishant Dogra,[1,*] Katrin Kroeger,[1] Rui Lin,[2] R. Chitra,[2] Tobias Donner,[1,†] and Tilman Esslinger[1]
[1]Institute for Quantum Electronics, ETH Zürich, 8093 Zürich, Switzerland
[2]Institute for Theoretical Physics, ETH Zürich, 8093 Zürich, Switzerland

(Received 13 August 2021; revised 22 February 2022; accepted 3 March 2022; published 8 April 2022)

We report on the experimental realization and detection of dynamical currents in a spin-textured lattice in momentum space. Collective tunneling is implemented via cavity-assisted Raman scattering of photons by a spinor Bose-Einstein condensate into an optical cavity. The photon field inducing the tunneling processes is subject to cavity dissipation, resulting in effective directional dynamics in a non-Hermitian setting. We observe that the individual tunneling events are superradiant in nature and locally resolve them in the lattice by performing real-time, frequency-resolved measurements of the leaking cavity field. The results can be extended to a regime exhibiting a cascade of currents and simultaneous coherences between multiple lattice sites, where numerical simulations provide further understanding of the dynamics. Our observations showcase dynamical tunneling in momentum-space lattices and provide prospects to realize dynamical gauge fields in driven-dissipative settings.

DOI: 10.1103/PhysRevLett.128.143602

Experiments with quantum degenerate atomic gases have successfully realized a wide variety of many-body lattice models, facilitating the exploration of complex out-of-equilibrium phenomena in highly controlled settings [1–3]. Engineering lattice bonds that dynamically depend on the local particle configuration is essential for simulating lattice gauge theories [4–6] and electron-phonon coupling [7,8]. Specifically, systems exhibiting density-dependent tunneling hold the potential to realize correlated many-body phenomena, such as pair superfluidity [9–11] and quantum scars [12,13]. So far, density-dependent tunneling in optical lattices has been implemented via periodic driving [14–19] or dipolar interactions [20], yet solely inferred from spectroscopic measurements or by comparison to theory. Here, we realize a complementary experimental scheme that allows us to engineer dynamical tunneling events in a momentum-space lattice and directly measure them in real-time.

Our implementation employs a spinor Bose-Einstein condensate (BEC) coupled to the fundamental mode of a high-finesse optical cavity by two transverse laser beams, see Fig. 1(a). Cavity-assisted Raman scattering transfers atoms between two spin levels ($|0\rangle$,$|1\rangle$), while imparting momentum to the BEC in multiples of the photon recoil [Figs. 1(b) and 1(c)]. This engenders spin and particle dynamics in a two-dimensional momentum grid, which we interpret as photon-assisted tunneling events in a synthetic lattice [21]. These events are mediated by an emergent cavity field, which self-consistently evolves with the atomic spin and density configuration. Hence, the tunneling rate dynamically depends on the buildup of coherences between neighboring sites, in contrast to experiments employing Bragg scattering from classical drives to control single-particle hopping rates in momentum lattices [22–24]. The underlying process is superradiant Raman scattering in an optical cavity [25,26], which is collectively enhanced by the number of participating emitters [27–32]. Since the resonator linewidth significantly exceeds site-to-site energy offsets, the cavity mode can accept different spectral components and mediate tunneling in a large momentum grid. The inherent dissipation due to cavity losses stimulates the superradiant transfers and renders the dynamics non-Hermitian. Making use of the cavity leakage, we gain nondestructive, real-time access to the atomic currents, which is often challenging in analog quantum simulations [33–35]. By performing frequency-resolved heterodyne measurements of the cavity field, we locally resolve the tunneling events in the momentum grid. A key feature of this implementation is that tunneling processes in opposite directions occur via different quantum paths and are independently controlled by the two drives. Our system constitutes a flexible platform to explore nonequilibrium lattice physics, thanks to the possibility to optically engineer dynamical currents and resolve them via the cavity field.

In our experiments, we prepare a BEC formed by $N \approx 10^5$ ^{87}Rb atoms in the $m_F = -1$ magnetic sublevel of the $F = 1$ hyperfine manifold. A magnetic field along the z direction generates a Zeeman splitting of $\omega_z = 2\pi \times 48$ MHz between the sublevels $m_F = -1$ and $m_F = 0$, which we label as $|0\rangle$ and $|1\rangle$, respectively. The atomic cloud is prepared inside an ultrahigh-finesse optical cavity with decay rate $\kappa = 2\pi \times 1.25$ MHz, and illuminated by two retroreflected laser fields far red-detuned from the atomic resonance. Their wavelength $\lambda = 784.7$ nm is associated with a recoil frequency of $\omega_{\mathrm{rec}} = 2\pi \times 3.73$ kHz.

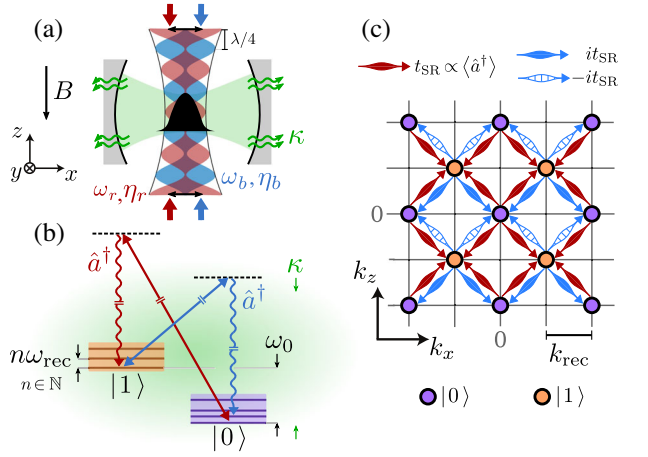

FIG. 1. Realization of dynamical currents in a momentum lattice. (a) Experimental setup. A BEC inside an optical cavity with decay rate κ is illuminated by two x-polarized, retroreflected Raman drives (red and blue) with frequencies $\omega_{r,b}$ and coupling strengths $\eta_{r,b}$. Their standing-wave modulations are shifted by $\lambda/4$. (b) Coupling scheme in a rotating frame at frequency $\bar{\omega}$. Raman scattering, involving absorption from the drives (solid arrows) and net emission of photons in the cavity mode (wiggly arrows and creation operator $\hat{a}^\dagger$), induces population transfer between specific momentum states of two different spin manifolds $|0\rangle$ (purple) and $|1\rangle$ (orange lines). These states are offset by the two-photon detuning ω_0 and by multiples of the recoil frequency ω_{rec}, with $\omega_{\mathrm{rec}} \leq \omega_0 \ll \kappa$. (c) Tunneling dynamics in a momentum grid. Raman scattering couples discrete momentum states of $|0\rangle$ (purple) and $|1\rangle$ (orange circles) differing by $\pm k_{\mathrm{rec}}$ in the x and z directions, giving rise to dynamical tunneling (red and blue arrows) with rate $t_{\mathrm{SR}} \propto \langle \hat{a}^\dagger \rangle$.

The frequencies of the drives $\omega_{r,b}$ lie on opposite sides of the dispersively shifted cavity resonance ω_c, with $\omega_b - \omega_c \approx \omega_z$ and $\omega_r - \omega_c \approx -\omega_z$. As shown in Fig. 1(a), their standing-wave modulations are shifted by $\lambda/4$ at the position of the atoms, such that the combined static lattice potential is fully erased for balanced laser powers [36].

This scheme realizes cavity-assisted Raman transitions between the spin states $|0\rangle$ and $|1\rangle$ with two-photon coupling rates $\eta_{r,b}$, cf. Fig. 1(b). We map the system to a tight-binding model in a rotating frame defined by the intermediate frequency of the two drives $\bar{\omega} = (\omega_b + \omega_r)/2$ [36], where the cavity detuning is defined as $\Delta_c = \bar{\omega} - \omega_c$. For balanced two-photon couplings $\eta = \eta_r = \eta_b$, the many-body Hamiltonian in momentum space $\hat{H} = \hat{H}_0 + \hat{H}_{t_{\mathrm{SR}}}$ contains a diagonal contribution

$$\hat{H}_0 = -\hbar\Delta_c \hat{a}^\dagger \hat{a} + \sum_{\substack{\{j,k\}\in\mathbb{Z} \\ \sigma\in\{0,1\}}} \hbar[\sigma\omega_0 + \omega^{\mathrm{kin}}_{(2j+\sigma,2k+\sigma)}] \hat{c}^{\sigma\dagger}_{(2j+\sigma,2k+\sigma)} \hat{c}^{\sigma}_{(2j+\sigma,2k+\sigma)}, \tag{1}$$

and a light-assisted tunneling term

$$\hat{H}_{t_{\mathrm{SR}}} = -\frac{\hbar\eta}{\sqrt{8}} \hat{a}^\dagger \sum_{\substack{\{j,k\}\in\mathbb{Z} \\ s_{1,2}=\pm 1}} [\hat{c}^{1\dagger}_{(2j+s_1,2k+s_2)} \hat{c}^{0}_{(2j,2k)} - i s_2 \hat{c}^{0\dagger}_{(2j,2k)} \hat{c}^{1}_{(2j+s_1,2k+s_2)}] + \mathrm{H.c.} \tag{2}$$

The bosonic operators $\hat{a}^\dagger$ and $\hat{c}^{\sigma\dagger}_{(l,m)}$ create photons in the fundamental mode of the cavity field and atoms in $|\sigma\rangle$ with (l,m) units of recoil momentum k_{rec} along (x,z) directions. We indicate the corresponding atomic modes in the momentum grid as $|l,m\rangle_\sigma$, with l, m being an even (odd) number for $\sigma = 0(1)$. The site-to-site energy offset results from a kinetic contribution $\omega^{\mathrm{kin}}_{(l,m)} = (l^2 + m^2)\omega_{\mathrm{rec}}$ and a global splitting between the spin manifolds $\omega_0 = (\omega_b - \omega_r)/2 - \omega_z$. This key feature allows us to resolve the emerging currents in the lattice by measuring the frequency of the corresponding cavity field. The Hamiltonian in Eq. (2) describes photon-mediated tunneling between next neighbors in the momentum grid with self-consistent rates $t_{\mathrm{SR}}(t) = -\eta\langle \hat{a}^\dagger(t)\rangle/\sqrt{8}$. The components of the atomic state tunneling in the $\pm z$ direction acquire a phase of $\mp i$ when scattering from the drive at ω_b, as depicted in Fig. 1(c). This is due to the relative spatial phase between the two standing-wave drives, which is also crucial for suppressing Bragg scattering within a spin sector along the z direction [21], e.g., between $|0,0\rangle_0$ and $|0,\pm 2\rangle_0$.

The system described by Eq. (2) is also a multilevel Tavis-Cummings model with collective coupling $\eta\sqrt{N/8}$. Since the experiment operates in an overdamped regime ($\kappa \gg \eta\sqrt{N/8}$), the system is strongly dissipative and decays through superradiant scattering when initialized in $|0,0\rangle_0$ [36,57,58]. In an illustrative picture, the evolution is primarily determined by Raman processes creating cavity photons ($\propto \hat{a}^\dagger$), as the opposite process of absorbing photons ($\propto \hat{a}$) is hindered by cavity losses. As a consequence, the non-Hermitian dynamics in the momentum lattice are directional, with preferred tunneling directions illustrated by the arrows in Fig. 1(c). The arising superradiant transfers are collectively enhanced, which results in tunneling rates evolving self-consistently with the coherences between the sites involved in each hopping process. This behavior is fundamentally different from the one observed in related experiments employing standing-wave Raman drives with equal spatial phase at the position of the BEC, where a low-momentum stable superradiant phase is created above a critical driving strength [59–61]. The large cavity linewidth ($\kappa \gg \omega_0, \omega_{\mathrm{rec}}$) facilitates tunneling in a large momentum grid, in contrast to potential implementations involving solely classical drives [21] or subrecoil cavities [62], where multiple lasers would be required.

In a first set of experiments, we prepare N atoms in the central lattice site $|0,0\rangle_0$ and characterize the first tunneling event, which populates a symmetric superposition of

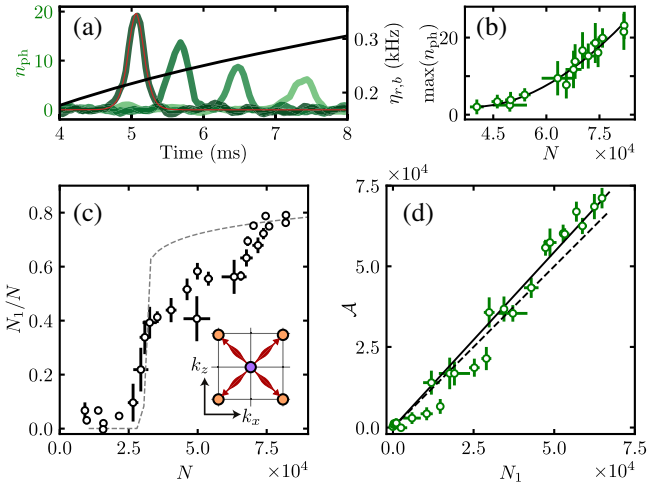

FIG. 2. Superradiant tunneling in the momentum lattice. (a) Representative photon pulses for different atom numbers $N = (8.1, 6.6, 4.9, 2.9) \times 10^4$ (darker to lighter green curves), together with a typical fit (red) [36] and coupling ramp η (black line). (b) Pulse amplitude versus N, with a power-law fit (black line) yielding an exponent of 1.8(3). (c) Transfer efficiency as a function of N. Dashed line: mean-field simulations [36]. Inset: sketch of the observed $|0,0\rangle_0 \rightarrow |\pm 1,\pm 1\rangle_1$ hopping. (d) One-to-one relation between the number of atoms N_1 in $|\pm 1,\pm 1\rangle_1$ and the photon pulse area $\mathcal{A}$, obtained by fitting the photon traces. A linear fit (solid) yields a slope of 1.09(2), compatible to the expectation of 1 (dashed line) within the combined systematic uncertainty due to photon (0.07) and atom number calibrations (0.04). Here, $\Delta_c = -2\pi \times 1.4(1)$ MHz and $\omega_0 = 2\pi \times 26(1)$ kHz. Throughout this Letter, the error bars represent the standard error of the mean.

nearest-neighboring sites $|\pm 1,\pm 1\rangle_1 = 1/2 \sum_{l,m=\pm 1} |l,m\rangle_1$. The strength of the drives is increased to $\eta = 2\pi \times 0.35(1)$ kHz within 10 ms and population transfer is signaled by a single pulse of the cavity field, cf. Fig. 2(a). We verify the superradiant nature of the scattered field by increasing the initial atom number N [63–65]. As a result, the light pulse occurs at shorter times and its amplitude increases superlinearly, cf. Fig. 2(b) [28,66]. We infer peak tunneling strengths ranging between $\max(|t_{\mathrm{SR}}|/2\pi) = 0.2(1)$–$0.4(1)$ kHz for different atom numbers. Tunneling occurs only above a finite atom number, which we attribute to the combined influence of residual spin dephasing and self-trapping due to finite contact interactions [23,36]. Accordingly, we reach transfer efficiencies of up to 0.8 [Fig. 2(c)], which are well captured by few-mode mean-field simulations [36]. The conservation of total angular momentum in the light-matter system leads to a one-to-one correspondence between the number of transferred atoms N_1 and the photon pulse area $\mathcal{A} = 2\kappa \int_0^\infty n_{\mathrm{ph}} dt$. We experimentally verify the relation $N_1 = \mathcal{A}$ [36] in Fig. 2(d).

Next, we further leverage on the real-time readout of the cavity field and demonstrate how frequency-resolved measurements allow us to localize the currents in the momentum grid. Around its peak value, the frequency of the cavity field ω_{01} (ω_{10}) associated with transitions from $|0\rangle$ to $|1\rangle$ ($|1\rangle$ to $|0\rangle$) follows from energy conservation

$$\omega_{\substack{01\\10}} - \bar{\omega} = \mp\, \omega_0 - [\omega^{\mathrm{kin}}(l_f, m_f) - \omega^{\mathrm{kin}}(l_i, m_i)], \quad (3)$$

where the indices l_i, m_i (l_f, m_f) label the initial (final) state of a given tunneling process [36]. In the rotating frame at $\bar{\omega}$, this corresponds to phase-modulated tunneling rates $t_{\mathrm{SR}} \propto \sqrt{n_{\mathrm{ph}}(t)} \exp(i\omega t)$ which remove ($\omega = \omega_{10} - \bar{\omega}$) or provide ($\omega = \omega_{01} - \bar{\omega}$) energy to reach different atomic configurations [67].

To assess this frequency dependence, we expose the system to stronger drives, which results in several superradiant tunneling events connecting multiple lattice sites. In Fig. 3(a), we present a representative spectrogram of the cavity field displaying three superradiant pulses, which we attribute to specific tunneling events in the momentum lattice. These are $|0,0\rangle_0 \rightarrow |\pm 1,\pm 1\rangle_1 \rightarrow |0,\mp 2\rangle_0 \rightarrow |\pm 1,\mp 1\rangle_1$, with $|0,\mp 2\rangle_0 = i/\sqrt{2}(|0,-2\rangle_0 - |0,2\rangle_0)$ and $|\pm 1,\mp 1\rangle_1 = -i/2 \sum_{l,m=\pm 1} m|l,m\rangle_1$, with the corresponding creation operators defined as $\hat{\psi}_j^\dagger$ ($j = \{0,1,3,2\}$) [36]. The observed frequencies of emission agree with Eq. (3) and with the results obtained from few-mode numerical simulations, see Fig. 3(e). We verify the involvement of the aforementioned states by performing spin-resolved measurements of the momentum distribution at different stages of the evolution [Figs. 3(b)–3(d)]. The observed population imbalance between states with $k_z > 0$ and $k_z < 0$ is attributed to spurious optical losses in the retroreflected path of the standing-wave drives (-z direction). We further benchmark the dynamics with *ab initio* Gross-Pitaevskii simulations (GPS) including the effects of the harmonic confinement and contact interactions [36]. The presence of tunneling terms with opposite signs ($\pm i t_{\mathrm{SR}}$) can give rise to destructive path interference when hopping towards inner sites in z direction. In particular, this effect is reflected in the suppressed hopping $|\pm 1,\pm 1\rangle_1 \nrightarrow |0,0\rangle_0$ [see Fig. 3(d)]. The emerging cavity field and the overall tunneling strength depend, in principle, on the sum of two-site coherences in Eq. (2) [36]. However, each tunneling event is associated with a well-defined spectral component of the cavity field fulfilling energy conservation. For sufficiently small tunneling rates ($|t_{\mathrm{SR}}| \ll \omega_{\mathrm{rec}}$), this field solely induces coherences between the corresponding adjacent lattice sites and the system exhibits local dynamical tunneling. This is reflected by the simulations of the coherences [Fig. 3(g)], which are compatible with the experimentally determined tunneling amplitudes $|t_{\mathrm{SR}}|$ associated with each of the superradiant pulses [see Fig. 3(f)].

The number of tunneling events can be extended by further increasing the coupling strength. As shown in Figs. 3(h) and 3(i), we observe up to seven superradiant transfers involving outer lattice sites, such as $|2,2\rangle_0$, which we identify by reading out the frequency of the cavity field and employing Eq. (3). The tunneling events are not

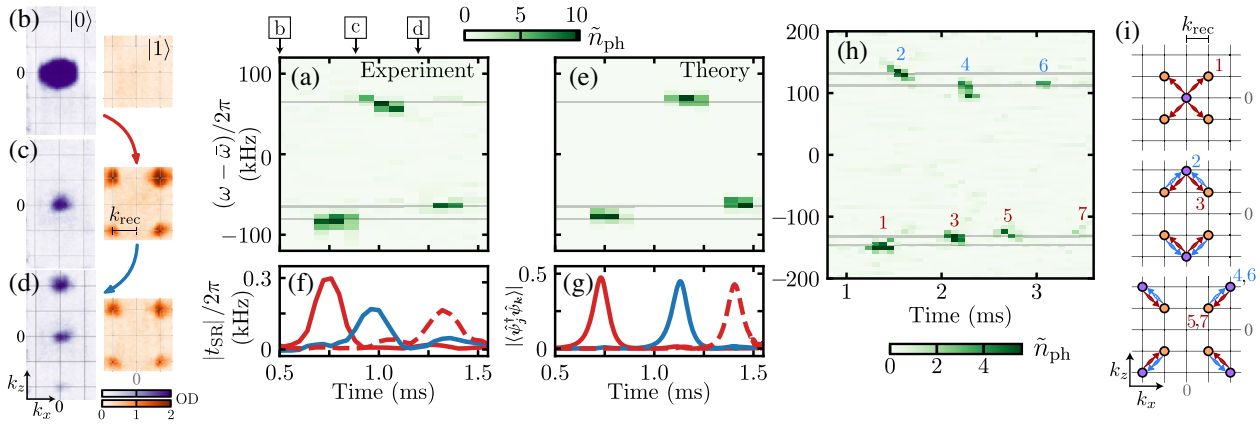

FIG. 3. Readout of lattice dynamics from the spectrum of the cavity field. (a) Representative photon number spectrogram $\tilde{n}(t,\omega)$ displaying time and frequency-resolved superradiant pulses. (b)–(d) Spin-resolved time-of-flight (TOF) images of the momentum distribution at different stages of the evolution [see square labels in (a)]. (e) Spectrogram obtained from mean-field simulations. (f) Experimental tunneling amplitudes $|t_{SR}|$, integrated in a $\delta\omega = 2\pi \times 5$ kHz window around the first (solid red), second (solid blue), and third photon peak (dashed red line) of the spectrogram in (a), respectively. (g) Corresponding simulated two-mode coherences $|\langle\hat{\psi}_1^\dagger\hat{\psi}_0\rangle|$, $|\langle\hat{\psi}_3^\dagger\hat{\psi}_1\rangle|$, and $|\langle\hat{\psi}_2^\dagger\hat{\psi}_3\rangle|$. (h) Spectrogram displaying multiple tunneling events, and (i) schematics of the inferred currents (1–7). The horizontal lines in the spectrograms indicate the pulse frequencies expected from Eq. (3). We prepare $N = 1.06(2) \times 10^5$ atoms in $|0\rangle$. For (a)–(d), the couplings are increased to $\eta = 2\pi \times 0.62(2)$ kHz within $t_{ramp} = 1.5$ ms, while $\Delta_c = -2\pi \times 0.7(2)$ MHz and $\omega_0 = 2\pi \times 72.5(5)$ kHz. For (h), $\eta = 2\pi \times 1.2(1)$ kHz, $t_{ramp} = 5$ ms, $\Delta_c = -2\pi \times 1.2(2)$ MHz, and $\omega_0 = 2\pi \times 139(4)$ kHz.

restricted to the shown processes as they arise from multiple competing quantum paths. A quantitative prediction in this regime goes beyond the scope of this Letter. We identify the following fundamental limitations to the number of tunneling events. First, in the absence of confining lattice potentials, the momentum states move out of the grid nodes due to oscillatory motion in the trap [22,68]. While for noninteracting systems this rate is solely determined by the trap frequencies ($\sim 2\pi \times 200$ Hz), our GPS indicate that repulsive contact interactions effectively increase the lifetime of the momentum lattice [36]. Second, heating of the BEC from off-resonant spontaneous emission progressively melts the momentum lattice when approaching the recoil temperature. However, this effect is negligible within the duration of our experiments.

The observations discussed so far involve independent tunneling events occurring sequentially in time. Our scheme can be extended to generate cascaded dynamics, where the tunneling events between different sites stimulate each other. We reduce the offset between the two spin manifolds to values comparable to the recoil frequency, shifting multiple states in the momentum lattice close to degeneracy [Fig. 4(a)]. In Fig. 4(b), we observe a single strong emission in the cavity field that is accompanied by several tunneling events within the pulse duration. Different from the results in Fig. 2(d), we observe an excess of detected photons in comparison to the population in $|\pm 1, \pm 1\rangle_1$, see Fig. 4(c). This effect is amplified as the emission frequency ω_p approaches the two-photon resonance ($\omega_p - \bar{\omega} \to 0$). Concurrently, we observe states with up to $10\hbar\omega_{rec}$ kinetic energy in the time-of-flight

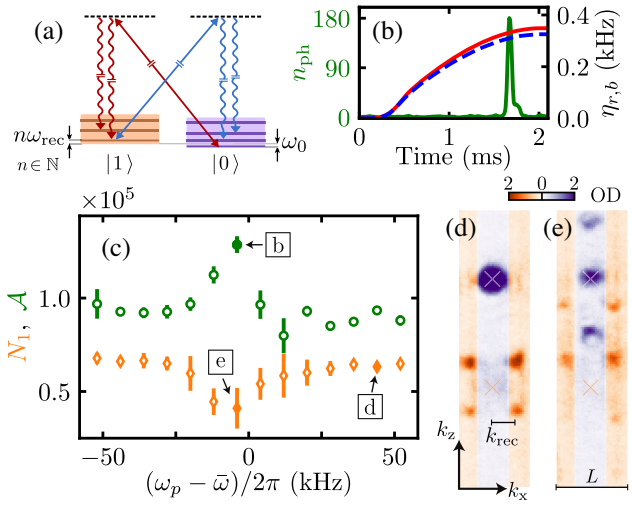

FIG. 4. Cascaded lattice dynamics. (a) Coupling scheme. The global splitting ω_0 is reduced below ω_{rec}, shifting several lattice sites close to degeneracy in the rotating frame. (b) Representative photon pulse (green). The couplings $\eta_{r,b}$ (red, blue curves) are increased with a small imbalance $\eta_r/(\eta_r + \eta_b) = 0.034(3)$. (c) Photon excess measurement. Pulse area $\mathcal{A}$ (circles) and final number of atoms N_1 in $|\pm 1, \pm 1\rangle_1$ (diamonds) as functions of ω_p. (d)–(e) Representative TOF images, with the white (orange) cross denoting the position of $|0,0\rangle_0$ ($|0,0\rangle_1$), which are separated by a Stern-Gerlach gradient along z. The purple (orange) color map indicates regions solely populated by atoms in $|0\rangle$ ($|1\rangle$). The small distance between the cavity mirrors $L \approx 175$ μm limits the both field of view along the x direction to $k_x \lesssim k_{rec}$. The square labels in (c) indicate the data points corresponding to panels (b),(d), and (e). For these measurements, $\Delta_c = -2\pi \times 3.4(2)$ MHz and $N = 9.1(1) \times 10^4$.

images [see Figs. 4(d) and 4(e)]. The GPS reproduce these results, helping to discern a cascade of hopping events towards outer lattice sites, in which the next tunneling starts before the previous one finishes [36]. These findings indicate that, within the duration of the cavity pulse, finite coherences between multiple lattice sites are simultaneously established, in contrast to the subsequent tunneling events at larger ω_0.

We experimentally demonstrated a scheme giving rise to self-consistent tunneling in a non-Hermitian momentum grid, engineered by superradiant Raman scattering of a spinor BEC coupled to an optical cavity. In particular, the tunneling rates evolve together with the coherences between the sites participating in each hopping event, which we locally resolve via frequency-selective measurements of the leaking cavity field. As an extension, the combination of real-time probing and continuous feedback acting on the phase of the drives [69] could facilitate the realization of nontrivial tunneling phases and pave the way to observe synthetic magnetic fields and topologically protected states in non-Hermitian settings [24,70,71]. In particular, an extension to running-wave Raman drives can result in emergent spin-orbit coupling [72–74]. Finally, exploring the interplay between cavity-assisted tunneling and Bose-Hubbard physics [75] holds the potential to realize unconventional strongly-correlated phases and dynamics [76–78].

We are grateful to A. Frank for electronic support, to M. Landini for discussions and early contributions to the project, and to K. Viebahn, A. U. J. Lode, and O. Zilberberg for fruitful discussions. We acknowledge computational time on the ETH Euler cluster. R. R-M., F. Ferri, F. Finger, T. D., and T. E. acknowledge funding from the Swiss National Science Foundation: Projects No. 182650 and No. 175329 (NAQUAS QuantERA) and NCCR QSIT (Grant No. 51NF40-185902), from EU Horizon2020: ERC advanced grant TransQ (Project No. 742579). R. L. and R. C. acknowledge funding from the ETH Grants.

R. R-M. and F. Ferri contributed equally to this work.

*Present address: Cavendish Laboratory, University of Cambridge, J. J. Thomson Avenue, Cambridge CB3 0HE, United Kingdom.

†donner@phys.ethz.ch

[1] T. Langen, R. Geiger, and J. Schmiedmayer, Ultracold atoms out of equilibrium, Annu. Rev. Condens. Matter Phys. **6**, 201 (2015).

[2] C. Gross and I. Bloch, Quantum simulations with ultracold atoms in optical lattices, Science **357**, 995 (2017).

[3] E. Altman *et al.*, Quantum simulators: Architectures and opportunities, PRX Quantum **2**, 017003 (2021).

[4] U.-J. Wiese, Ultracold quantum gases and lattice systems: Quantum simulation of lattice gauge theories, Ann. Phys. (Berlin) **525**, 777 (2013).

[5] E. Zohar, J. I. Cirac, and B. Reznik, Quantum simulations of lattice gauge theories using ultracold atoms in optical lattices, Rep. Prog. Phys. **79**, 014401 (2015).

[6] V. Kasper, G. Juzeliūnas, M. Lewenstein, F. Jendrzejewski, and E. Zohar, From the Jaynes–Cummings model to non-Abelian gauge theories: A guided tour for the quantum engineer, New J. Phys. **22**, 103027 (2020).

[7] U. Bissbort, D. Cocks, A. Negretti, Z. Idziaszek, T. Calarco, F. Schmidt-Kaler, W. Hofstetter, and R. Gerritsma, Emulating Solid-State Physics with a Hybrid System of Ultracold Ions and Atoms, Phys. Rev. Lett. **111**, 080501 (2013).

[8] F. Giustino, Electron-phonon interactions from first principles, Rev. Mod. Phys. **89**, 015003 (2017).

[9] M. Eckholt and J. J. García-Ripoll, Correlated hopping of bosonic atoms induced by optical lattices, New J. Phys. **11**, 093028 (2009).

[10] A. Rapp, X. Deng, and L. Santos, Ultracold Lattice Gases with Periodically Modulated Interactions, Phys. Rev. Lett. **109**, 203005 (2012).

[11] M. DiLiberto, C. E. Creffield, G. I. Japaridze, and C. MoraisSmith, Quantum simulation of correlated-hopping models with fermions in optical lattices, Phys. Rev. A **89**, 013624 (2014).

[12] H. Zhao, J. Vovrosh, F. Mintert, and J. Knolle, Quantum Many-Body Scars in Optical Lattices, Phys. Rev. Lett. **124**, 160604 (2020).

[13] A. Hudomal, I. Vasić, N. Regnault, and Z. Papić, Quantum scars of bosons with correlated hopping, Commun. Phys. **3**, 99 (2020).

[14] R. Ma, M. E. Tai, P. M. Preiss, W. S. Bakr, J. Simon, and M. Greiner, Photon-Assisted Tunneling in a Biased Strongly Correlated Bose Gas, Phys. Rev. Lett. **107**, 095301 (2011).

[15] F. Meinert, M. J. Mark, K. Lauber, A. J. Daley, and H.-C. Nägerl, Floquet Engineering of Correlated Tunneling in the Bose-Hubbard Model with Ultracold Atoms, Phys. Rev. Lett. **116**, 205301 (2016).

[16] W. Xu, W. Morong, H.-Y. Hui, V. W. Scarola, and B. DeMarco, Correlated spin-flip tunneling in a Fermi lattice gas, Phys. Rev. A **98**, 023623 (2018).

[17] L. W. Clark, B. M. Anderson, L. Feng, A. Gaj, K. Levin, and C. Chin, Observation of Density-Dependent Gauge Fields in a Bose-Einstein Condensate Based on Micromotion Control in a Shaken Two-Dimensional Lattice, Phys. Rev. Lett. **121**, 030402 (2018).

[18] F. Görg, K. Sandholzer, J. Minguzzi, R. Desbuquois, M. Messer, and T. Esslinger, Realization of density-dependent Peierls phases to engineer quantized gauge fields coupled to ultracold matter, Nat. Phys. **15**, 1161 (2019).

[19] C. Schweizer, F. Grusdt, M. Berngruber, L. Barbiero, E. Demler, N. Goldman, I. Bloch, and M. Aidelsburger, Floquet approach to $\mathbb{Z}2$ lattice gauge theories with ultracold atoms in optical lattices, Nat. Phys. **15**, 1168 (2019).

[20] S. Baier, M. J. Mark, D. Petter, K. Aikawa, L. Chomaz, Z. Cai, M. Baranov, P. Zoller, and F. Ferlaino, Extended Bose-Hubbard models with ultracold magnetic atoms, Science **352**, 201 (2016).

[21] B. Gadway, Atom-optics approach to studying transport phenomena, Phys. Rev. A **92**, 043606 (2015).

[22] E. J. Meier, F. A. An, and B. Gadway, Atom-optics simulator of lattice transport phenomena, Phys. Rev. A **93**, 051602(R) (2016).
[23] F. A. An, E. J. Meier, J. Ang'ong'a, and B. Gadway, Correlated Dynamics in a Synthetic Lattice of Momentum States, Phys. Rev. Lett. **120**, 040407 (2018).
[24] W. Gou, T. Chen, D. Xie, T. Xiao, T.-S. Deng, B. Gadway, W. Yi, and B. Yan, Tunable Nonreciprocal Quantum Transport through a Dissipative Aharonov-Bohm Ring in Ultracold Atoms, Phys. Rev. Lett. **124**, 070402 (2020).
[25] G. Vrijsen, O. Hosten, J. Lee, S. Bernon, and M. A. Kasevich, Raman Lasing with a Cold Atom Gain Medium in a High-Finesse Optical Cavity, Phys. Rev. Lett. **107**, 063904 (2011).
[26] J. G. Bohnet, Z. Chen, J. M. Weiner, D. Meiser, M. J. Holland, and J. K. Thompson, A steady-state superradiant laser with less than one intracavity photon, Nature (London) **484**, 78 (2012).
[27] R. H. Dicke, Coherence in spontaneous radiation processes, Phys. Rev. **93**, 99 (1954).
[28] M. Gross and S. Haroche, Superradiance: An essay on the theory of collective spontaneous emission, Phys. Rep. **93**, 301 (1982).
[29] D. Schneble, G. K. Campbell, E. W. Streed, M. Boyd, D. E. Pritchard, and W. Ketterle, Raman amplification of matter waves, Phys. Rev. A **69**, 041601(R) (2004).
[30] Y. Yoshikawa, T. Sugiura, Y. Torii, and T. Kuga, Observation of superradiant Raman scattering in a Bose-Einstein condensate, Phys. Rev. A **69**, 041603(R) (2004).
[31] M. M. Cola and N. Piovella, Theory of collective Raman scattering from a Bose-Einstein condensate, Phys. Rev. A **70**, 045601 (2004).
[32] T. Wang and S. F. Yelin, Theory for Raman superradiance in atomic gases, Phys. Rev. A **72**, 043804 (2005).
[33] C. Laflamme, D. Yang, and P. Zoller, Continuous measurement of an atomic current, Phys. Rev. A **95**, 043843 (2017).
[34] D. Yang, C. Laflamme, D. V. Vasilyev, M. A. Baranov, and P. Zoller, Theory of a Quantum Scanning Microscope for Cold Atoms, Phys. Rev. Lett. **120**, 133601 (2018).
[35] K. T. Geier, J. Reichstetter, and P. Hauke, Non-invasive measurement of currents in analog quantum simulators, arXiv:2106.12599.
[36] See Supplemental Material at http://link.aps.org/supplemental/10.1103/PhysRevLett.128.143602 for experimental and theoretical details, which includes Refs. [37–56].
[37] B. Gadway, D. Pertot, R. Reimann, M. G. Cohen, and D. Schneble, Analysis of Kapitza-Dirac diffraction patterns beyond the Raman-Nath regime, Opt. Express **17**, 19173 (2009).
[38] F. Le Kien, P. Schneeweiss, and A. Rauschenbeutel, Dynamical polarizability of atoms in arbitrary light fields: General theory and application to cesium, Eur. Phys. J. D **67**, 92 (2013).
[39] M. Landini, N. Dogra, K. Kroeger, L. Hruby, T. Donner, and T. Esslinger, Formation of a Spin Texture in a Quantum Gas Coupled to a Cavity, Phys. Rev. Lett. **120**, 223602 (2018).
[40] N. Dogra, M. Landini, K. Kroeger, L. Hruby, T. Donner, and T. Esslinger, Dissipation-induced structural instability and chiral dynamics in a quantum gas, Science **366**, 1496 (2019).
[41] G. Reinaudi, T. Lahaye, Z. Wang, and D. Guéry-Odelin, Strong saturation absorption imaging of dense clouds of ultracold atoms, Opt. Lett. **32**, 3143 (2007).
[42] N. Goldman, G. Juzeliūnas, P. Öhberg, and I. B. Spielman, Light-induced gauge fields for ultracold atoms, Rep. Prog. Phys. **77**, 126401 (2014).
[43] D. M. Stamper-Kurn and M. Ueda, Spinor Bose gases: Symmetries, magnetism, and quantum dynamics, Rev. Mod. Phys. **85**, 1191 (2013).
[44] T. Chen, D. Xie, B. Gadway, and B. Yan, A Gross-Pitaevskii-equation description of the momentum-state lattice: Roles of the trap and many-body interactions, arXiv:2103.14205.
[45] F. A. An, B. Sundar, J. Hou, X.-W. Luo, E. J. Meier, C. Zhang, K. R. A. Hazzard, and B. Gadway, Nonlinear Dynamics in a Synthetic Momentum-State Lattice, Phys. Rev. Lett. **127**, 130401 (2021).
[46] L. Deng, E. W. Hagley, J. Wen, M. Trippenbach, Y. Band, P. S. Julienne, J. E. Simsarian, K. Helmerson, S. L. Rolston, and W. D. Phillips, Four-wave mixing with matter waves, Nature (London) **398**, 218 (1999).
[47] L. F. Shampine and M. W. Reichelt, The MATLAB ODE suite, SIAM J. Sci. Comput. **18**, 1 (1997).
[48] A. U. J. Lode, Multiconfigurational time-dependent Hartree method for bosons with internal degrees of freedom: Theory and composite fragmentation of multicomponent Bose-Einstein condensates, Phys. Rev. A **93**, 063601 (2016).
[49] O. E. Alon, A. I. Streltsov, and L. S. Cederbaum, Multiconfigurational time-dependent Hartree method for bosons: Many-body dynamics of bosonic systems, Phys. Rev. A **77**, 033613 (2008).
[50] E. Fasshauer and A. U. J. Lode, Multiconfigurational time-dependent Hartree method for fermions: Implementation, exactness, and few-fermion tunneling to open space, Phys. Rev. A **93**, 033635 (2016).
[51] R. Lin, P. Molignini, L. Papariello, M. C. Tsatsos, C. Lévêque, S. E. Weiner, E. Fasshauer, R. Chitra, and A. U. J. Lode, MCTDH-X: The multiconfigurational time-dependent Hartree method for indistinguishable particles software, Quantum Sci. Technol. **5**, 024004 (2020).
[52] A. U. J. Lode, C. Lévêque, L. B. Madsen, A. I. Streltsov, and O. E. Alon, Colloquium: Multiconfigurational time-dependent Hartree approaches for indistinguishable particles, Rev. Mod. Phys. **92**, 011001 (2020).
[53] A. U. J. Lode, M. C. Tsatsos, E. Fasshauer, R. Lin, L. Papariello, P. Molignini, C. Lévêque, and S. E. Weiner, MCTDH-X: The time-dependent multiconfigurational Hartree for indistinguishable particles software (2021), http://ultracold.org.
[54] M.-O. Mewes, M. R. Andrews, N. J. van Druten, D. M. Kurn, D. S. Durfee, C. G. Townsend, and W. Ketterle, Collective Excitations of a Bose-Einstein Condensate in a Magnetic Trap, Phys. Rev. Lett. **77**, 988 (1996).
[55] F. Dalfovo, S. Giorgini, L. P. Pitaevskii, and S. Stringari, Theory of Bose-Einstein condensation in trapped gases, Rev. Mod. Phys. **71**, 463 (1999).
[56] F. Chevy, V. Bretin, P. Rosenbusch, K. W. Madison, and J. Dalibard, Transverse Breathing Mode of an Elongated Bose-Einstein Condensate, Phys. Rev. Lett. **88**, 250402 (2002).

[57] J. Fan, G. Chen, and S. Jia, Atomic self-organization emerging from tunable quadrature coupling, Phys. Rev. A **101**, 063627 (2020).

[58] R. Lin, R. Rosa-Medina, F. Ferri, F. Finger, K. Kroeger, T. Donner, T. Esslinger, and R. Chitra, Dissipation-engineered family of nearly dark states in many-body cavity-atom systems, Phys. Rev. Lett. **128**, 153601 (2022).

[59] R. M. Kroeze, Y. Guo, V. D. Vaidya, J. Keeling, and B. L. Lev, Spinor Self-Ordering of a Quantum Gas in a Cavity, Phys. Rev. Lett. **121**, 163601 (2018).

[60] F. Ferri, R. Rosa-Medina, F. Finger, N. Dogra, M. Soriente, O. Zilberberg, T. Donner, and T. Esslinger, Emerging Dissipative Phases in a Superradiant Quantum Gas with Tunable Decay, Phys. Rev. X **11**, 041046 (2021).

[61] F. Mivehvar, F. Piazza, T. Donner, and H. Ritsch, Cavity QED with quantum gases: new paradigms in many-body physics, Adv. Phys. **70**, 1 (2021).

[62] H. Keßler, J. Klinder, M. Wolke, and A. Hemmerich, Optomechanical atom-cavity interaction in the sub-recoil regime, New J. Phys. **16**, 053008 (2014).

[63] M. A. Norcia, M. N. Winchester, J. R. K. Cline, and J. K. Thompson, Superradiance on the millihertz linewidth strontium clock transition, Sci. Adv. **2**, e1601231 (2016).

[64] T. Laske, H. Winter, and A. Hemmerich, Pulse Delay Time Statistics in a Superradiant Laser with Calcium Atoms, Phys. Rev. Lett. **123**, 103601 (2019).

[65] G. Ferioli, A. Glicenstein, F. Robicheaux, R. T. Sutherland, A. Browaeys, and I. Ferrier-Barbut, Laser-Driven Superradiant Ensembles of Two-Level Atoms near Dicke Regime, Phys. Rev. Lett. **127**, 243602 (2021).

[66] L. Mandel, E. Wolf, and C. U. Press, *Optical Coherence and Quantum Optics*, EBL-Schweitzer (Cambridge University Press, Cambridge, England, 1995).

[67] C. Sias, H. Lignier, Y. P. Singh, A. Zenesini, D. Ciampini, O. Morsch, and E. Arimondo, Observation of Photon-Assisted Tunneling in Optical Lattices, Phys. Rev. Lett. **100**, 040404 (2008).

[68] F. A. An, The cold atom toolbox in momentum space, Ph.D. thesis, University of Illinois at Urbana-Champaign, 2020.

[69] K. Kroeger, N. Dogra, R. Rosa-Medina, M. Paluch, F. Ferri, T. Donner, and T. Esslinger, Continuous feedback on a quantum gas coupled to an optical cavity, New J. Phys. **22**, 033020 (2020).

[70] Z. Gong, Y. Ashida, K. Kawabata, K. Takasan, S. Higashikawa, and M. Ueda, Topological Phases of Non-Hermitian Systems, Phys. Rev. X **8**, 031079 (2018).

[71] T. Ozawa and H. M. Price, Topological quantum matter in synthetic dimensions, Nat. Rev. Phys. **1**, 349 (2019).

[72] R. M. Kroeze, Y. Guo, and B. L. Lev, Dynamical Spin-Orbit Coupling of a Quantum Gas, Phys. Rev. Lett. **123**, 160404 (2019).

[73] C.-M. Halati, A. Sheikhan, and C. Kollath, Cavity-induced spin-orbit coupling in an interacting bosonic wire, Phys. Rev. A **99**, 033604 (2019).

[74] S. Ostermann, H. Ritsch, and F. Mivehvar, Many-body phases of a planar Bose-Einstein condensate with cavity-induced spin-orbit coupling, Phys. Rev. A **103**, 023302 (2021).

[75] R. Landig, L. Hruby, N. Dogra, M. Landini, R. Mottl, T. Donner, and T. Esslinger, Quantum phases from competing short- and long-range interactions in an optical lattice, Nature (London) **532**, 476 (2016).

[76] C.-M. Halati, A. Sheikhan, and C. Kollath, Cavity-induced artificial gauge field in a Bose-Hubbard ladder, Phys. Rev. A **96**, 063621 (2017).

[77] T. Chanda, R. Kraus, G. Morigi, and J. Zakrzewski, Self-organized topological insulator due to cavity-mediated correlated tunneling, Quantum **5**, 501 (2021).

[78] E. Colella, F. Mivehvar, and H. Ritsch, Open Quantum-System Simulation of Faraday's Induction Law via Dynamical Instabilities, Phys. Rev. Lett. **128**, 070603 (2022).